Vehicle System Dynamics
2002, Vol. 38, No. 3, pp. 211–242

0042-3114/02/3803-211$16.00

Vehicle Handling Improvement by Active Steering

SAÏD MAMMAR[1] AND DAMIEN KOENIG[2]

SUMMARY

This paper first analyses some stability aspects of vehicle lateral motion, then a coprime factors and linear fractional transformations (LFT) based feedforward and feedback H_∞ control for vehicle handling improvement is presented. The control synthesis procedure uses a linear vehicle model which includes the yaw motion and disturbance input with speed and road adhesion variations. The synthesis procedure allows the separate processing of the driver reference signal and robust stabilization problem or disturbance rejection. The control action is applied as an additional steering angle, by combination of the driver input and feedback of the yaw rate. The synthesized controller is tested for different speeds and road conditions on a nonlinear model in both disturbance rejection and driver imposed yaw reference tracking maneuvers.

NOMENCLATURE

G	vehicle center of gravity (CG)
m, J	mass and inertia (991 kg, 1574 kg m^2)
l_f	distance from CG to front axle (1.00 m)
l_r	distance from CG to rear axle (1.46 m)
s_b	wheel-base (1.40 m)
R	steering gear ratio (21)
c_f	front cornering stiffness (41.6 kN/rad)
c_r	rear cornering stiffness (47.13 kN/rad)
μ	road adhesion (scaling factor $[0, 1]$)
n_t	tire-road length contact (1.3 cm)
f_{x_i}, f_{y_i}	longitudinal and lateral forces of the ith tire
f_{xf}, f_{yf}	total front longitudinal and lateral force

[1]Address correspondence to: Saïd Mammar, CEMIF-LSC, Laboratoire de Systèmes Complexes, Université d'Évry Val-d'Essonne and INRETS/LIVIC, Institut National de Recherche sur les Transports et leur sécurité, 2 avenue du Général Malleret Joinville, 94114 Arcueil cedex, France. Tel.: 33-1 40 43 29 08; Fax: 33-1 40 43 29 30; E-mail: said.mammar@inrets.fr
[2]LAG, Laboratoire d'Automatique de Grenoble, UMR CNRS-INPG-UJF, BP 46, 38402 Saint Martin D'hères cedex, France. E-mail: koenig@esisar.inpg.fr

f_{xr}, f_{yr}	total rear longitudinal and lateral force
α_i	slip angle of the ith tire (rad)
$w = f_w$	wind force (N)
l_w	distance of wind force action (0.40 m)
k_x, k_y	long. and lateral air drag coefficients
(v_x, v_y)	CG speed written in vehicle frame
β	vehicle sideslip angle
r	yaw rate
$u = \delta_f$	steering angle

1. INTRODUCTION

Vehicle handling improvement has received much attention from the research community and car manufacturers during the last decade. Presently, vehicle stability enhancement techniques use only the available functions of braking and traction components in aiding driver during maneuvers. However as pointed in [13], active steering has attractive benefits with regard to vehicle handling improvement. For example, front wheels active steering leads to additional lateral forces which can be used in order to reject yaw and roll torque disturbances that rise from μ split but also from asymmetric braking or wind forces and this even on decreased road adhesion conditions. Active steering has also application in rollover avoidance for vehicles with elevated center of gravity [2]. Active steering of 2-wheel steering vehicles has been principally studied by Ackerman. In [3], an analytical method which allows robust unilateral decoupling of the yaw rate from the lateral dynamics has been presented. The controller output consists in an additional steering angle obtained by integration of the difference between the reference yaw rate value as commanded by the driver and the actual achieved vehicle yaw rate. Several refinements have been introduced in [4], in order to improve vehicle handling while ensuring similar steady state behavior for both the controlled and the conventional cars.

In this paper, a vehicle handling scheme is developed using a combination of feedforward and feedback controllers. The controller feedbacks the yaw rate sensor and adds a feedforward action as a function of the driver steering command. This configuration allows robust model matching against parameters variations and rejection of lateral forces and torque disturbances. The controller configuration also allows a simple and a direct implementation on actual electrically steered vehicles. Control synthesis is conducted on an LFT model [5, 6] in order to represent vehicle speed and road adhesion variations while simulation tests are conducted on a nonlinear model.

The paper is organized as follows: Section 2 introduces the car models used for active steering controller synthesis and analysis. Some stability aspects are discussed

and an LFT model is developed in order to represent system parameter variations. Active steering objectives and synthesis methodology are presented in Section 3 which ends with controller implementation. Simulation results for typical maneuvers are provided in Section 4.

2. VEHICLE LATERAL DYNAMICS MODELLING AND ANALYSIS

2.1. Nonlinear Model

As we are only concerned with lateral control, a simple nonlinear model of a vehicle is derived by neglecting heave, roll and pitch motions. This model includes the two translational motions and the yaw motion. According to Figure 1, the vehicle wheels are numbered from 1 to 4. The interaction between the tire i ($i = 1, 2, 3, 4$) and road surface is decomposed into longitudinal forces $f_{x_i}(\lambda_i)$ and lateral forces $f_{y_i}(\alpha_i)$. These forces will be detailed below. The nonlinear model is obtained by writing the translational and rotational equations in the vehicle fixed frame

$$\begin{cases} m\left(\dot{v}_x - v_y r\right) = f_{x_f}\cos\delta_f + f_{x_r} - f_{y_f}\sin\delta_f - k_x v_x|v_x| \\ m\left(\dot{v}_y + v_x r\right) = f_{x_f}\sin\delta_f + f_{y_r} + f_{y_f}\cos\delta_f - k_y v_y|v_y| + f_w \\ J\dot{r} = l_f\left(f_{x_f}\sin\delta_f + f_{y_f}\cos\delta_f\right) - l_r f_{y_r} + \dfrac{s_b}{2}\left(\Delta f_x - \Delta f_{y_f}\sin\delta_f\right) + l_w f_w \end{cases} \tag{1}$$

where

$$\begin{aligned} f_{x_f} &= f_{x_1} + f_{x_2} & f_{y_f} &= f_{y_1} + f_{y_2} \\ f_{x_r} &= f_{x_3} + f_{x_4} & f_{y_r} &= f_{y_3} + f_{y_4} \\ \Delta f_x &= (f_{x_4} - f_{x_3}) + (f_{x_2} - f_{x_1})\cos\delta_f \approx 0 & \Delta f_{y_f} &= f_{y_2} - f_{y_1} \end{aligned}$$

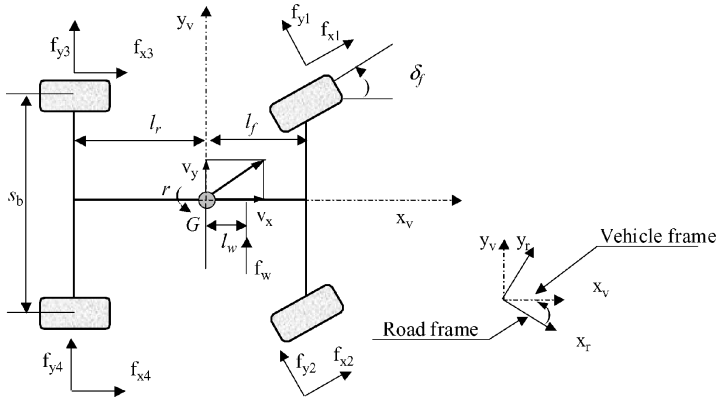

Fig. 1. Vehicle and external forces.

Table 1. Nonlinear formulas of tire slip angles.

$$\alpha_1 = \delta_f - \tan^{-1}\left(\frac{v_y - (n_t\cos\delta_f)\dot{\delta}_f - (n_t\cos\delta_f - l_f)r}{v_x + (n_t\sin\delta_f)\dot{\delta}_f + \left(n_t\sin\delta_f - \frac{s_b}{2}\right)r}\right)$$

$$\alpha_2 = \delta_f - \tan^{-1}\left(\frac{v_y - (n_t\cos\delta_f)\dot{\delta}_f - (n_t\cos\delta_f - l_f)r}{v_x + (n_t\sin\delta_f)\dot{\delta}_f + \left(n_t\sin\delta_f + \frac{s_b}{2}\right)r}\right)$$

$$\alpha_3 = -\tan^{-1}\left(\frac{v_y - l_r r}{v_x - \frac{s_b r}{2}}\right)$$

$$\alpha_4 = -\tan^{-1}\left(\frac{v_y - l_r r}{v_x + \frac{s_b r}{2}}\right)$$

The distances, the longitudinal and lateral forces are appearing on Figure 1. The nominal values and range of the parameters are given in the nomenclature at the beginning of the paper. They correspond to an understeering medium class European passenger car.

The longitudinal forces depend directly on the tire slip coefficient (λ_i), while the lateral forces depend on the tire slip angles (α_i). Table 1 summarizes the expressions of the tire slip angles. The longitudinal slip of the tire is not considered here. The longitudinal forces are only calculated in order to maintain a quasi constant forward speed. Several models that describe with relative accuracy the complex phenomena of the tire-road contact exist. Linear models that use different cornering stiffnesses for the front and rear tires are generally sufficient for motorway driving conditions under assumptions of small angles. Otherwise, nonlinear models may be used when high angles values or tire forces saturation are expected. These models are both static maps [7, 8] and dynamics [9]. In this paper, the magic formula of Pacejka is used for each tire in order to determine the lateral forces [10].

$$f_{yi}(\alpha_i) = d_i \sin\left[c_i \tan^{-1}\left\{b_i(1-e_i)\alpha_i + e_i \tan^{-1}(b_i\alpha_i)\right\}\right] \tag{2}$$

The coefficients b_i, c_f, d_i, e_i depend on the tire characteristics, on the road conditions, and on the vehicle operational conditions. Parameters values when road friction is high are given in Table 2.

Let μ be a common road adhesion coefficient with $\mu = 0.2$ for icy road and $\mu = 1$ for nominal road adhesion. The influence of the road adhesion on the lateral forces is incorporated in the magic formula by changing b_i to $(2-\mu)b_i$, c_i to $\left(\frac{5}{4} - \frac{\mu}{4}\right)c_i$ and d_i to μd_i.

Table 2. Tire model parameters on high friction road.

Tire	b_i	c_i	d_i	e_i
Front $(i = 1, 2)$	8.3278	1.1009	2268.0	−1.661
Rear $(i = 3, 4)$	11.6590	1.1009	1835.8	−1.542

Vehicle trajectories are now simulated with respect to various initial conditions, steering command, road adhesion and speed, in order to evaluate vehicle stability domain and kind of instability that may occur.

2.2. Nonlinear Model Analysis

It has been shown in [11] that the magic formula is sufficient to prove that the vehicle may go into spin, thus become unstable, for some initial conditions or large steering angle input on low adhesion road.

In this first simulations set, the forward speed is equal to 20 m/s. Stable trajectories are in solid lines while unstable ones are in dashed lines. One can see from Figure 2 that when the steering angle is zero, any vehicle initial condition (x) converges to the origin when the road adhesion is maximal. However on low friction road

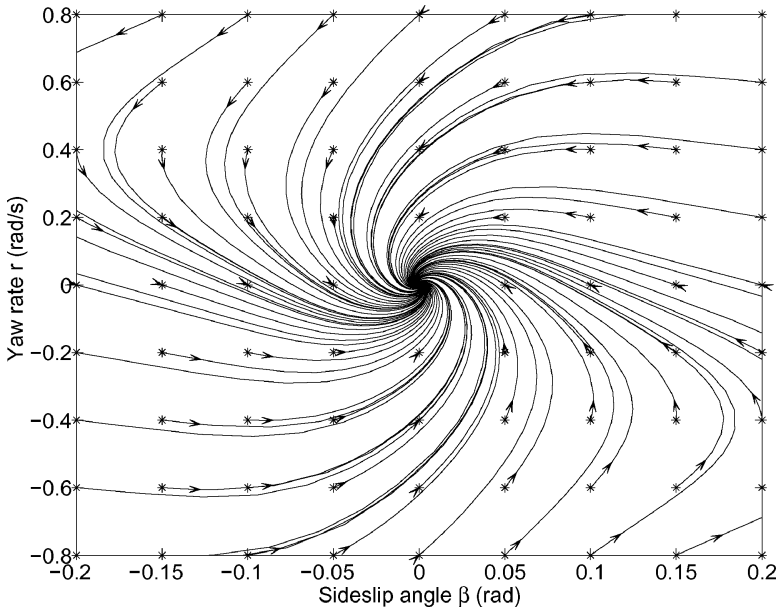

Fig. 2. State trajectories at nominal road adhesion and zero steering angle.

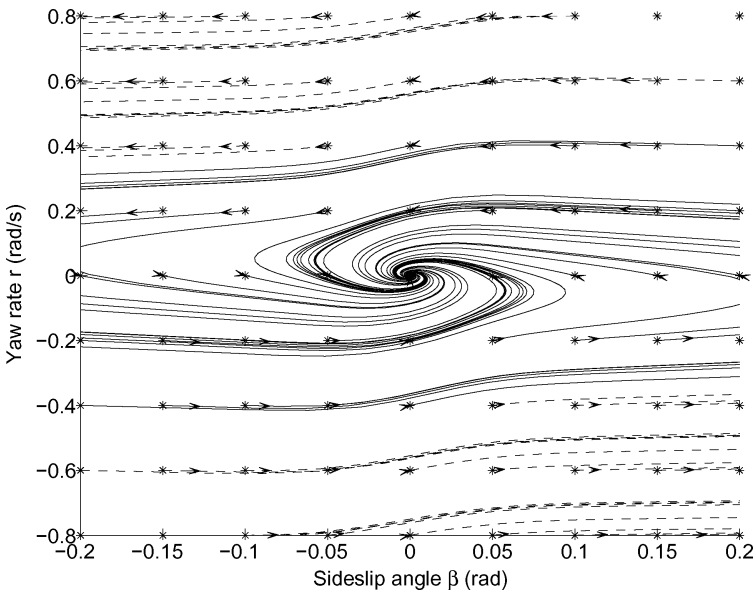

Fig. 3. State trajectories at low road adhesion μ and zero steering angle.

($\mu = 0.3$), some initial conditions lead to vehicle spin as the sideslip angle diverges (Fig. 3).

On the other hand, Figure 4 shows that on low friction road, large steering angles lead also to vehicle spin and reduction of the stability region.

In Figures 5 and 6, the effect of speed and road adhesion are examined. The steering angle command in Figure 5 is zero while in Figure 6, it is constant and is equal to 0.05 rad. In both cases, the vehicle initial state is $[\beta_0, r_0]^T = [0.15, 0.5]^T$. The speed is varying from 1 m/s to 50 m/s, while four road adhesion coefficients are considered $\{\mu = 0.2, 0.4, 0.6, 0.8\}$. For the sake of clarity, trajectories are only plotted from 5 m/s and every 5 m/s. Figures 5(a) and 6(a) show that for $\mu = 0.2$, only the speed 5 m/s is still stable. On Figures 5(b) and 6(b), only speeds greater or equal 40 m/s and 20 m/s are unstable respectively, while Figures 5(c–d) and 6(c–d) show that all speeds are stable for μ greater or equal 0.6. These Figures also point out that some trajectories that are stable for zero steering angle become unstable when a constant non zero steering angle is considered.

Performing a more extensive simulation, a vehicle stable operating domain may be constructed for these initial conditions in the (speed, road adhesion) plane (Figs. 7 and 8). Star markers are used for the stable points and dotted markers are used for the unstable ones. From these figures, one can also notice the reduction of the stability

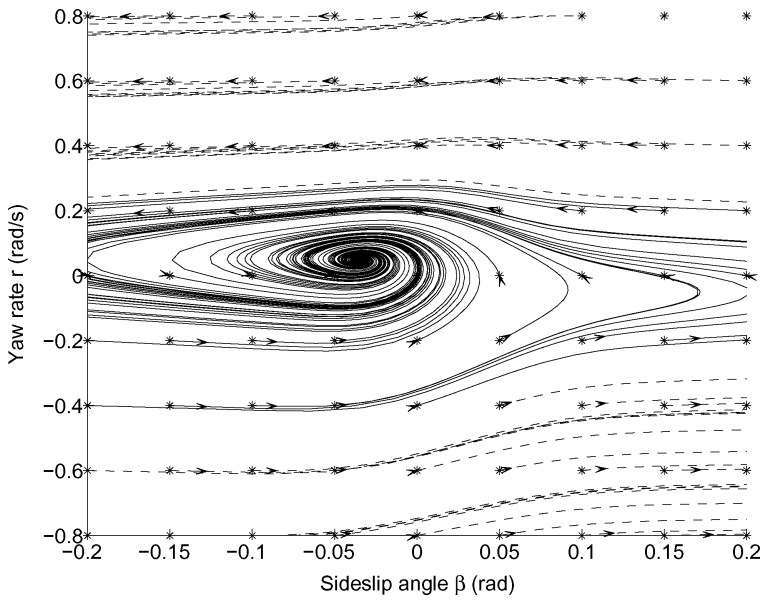

Fig. 4. State trajectories at low road adhesion μ and $\delta_f = 0.05$ rad.

domain, due to the driver steering angle input. This reduction becomes more pronounced when the steering angle increases.

This non-linear model is used for controller analysis, but for synthesis purposes, linearization of (2) about $\alpha_i = 0$ is used. This leads to $f_{y_i}(\alpha_i) = (d_i c_i b_i)\alpha_i$.

2.3. Nominal Linear Model

The model used for control synthesis is derived from the previous model in which the longitudinal velocity is assumed to be constant ($v_x = v, \dot{v}_x = 0$), and all the angles are assumed to be small [12]. The sideslip angle $\left(\beta = \frac{v_y}{v}\right)$ is used as a state variable. It is also assumed equal cornering stiffnesses for the two front wheels $\left(\frac{c_f}{2} = d_1 c_1 b_1 = d_2 c_2 b_2\right)$ and the rear ones $\left(\frac{c_r}{2} = d_3 c_3 b_3 = d_4 c_4 b_4\right)$. When the track width is neglected, the tire slip angles are reduced to $\left(\alpha_f = \alpha_1 = \alpha_2\right)$ and $(\alpha_r = \alpha_3 = \alpha_4)$. These angles are also considered small and thus the total front and rear lateral forces $f_{y_f}(\alpha_f)$ and $f_{y_r}(\alpha_r)$ are respectively given by

$$f_{y_f}(\alpha_f) = f_{y_1} + f_{y_2} = c_f\left(\delta_f - \beta - \frac{l_f}{v} r\right) \tag{3}$$

$$f_{y_r}(\alpha_r) = f_{y_3} + f_{y_4} = -c_r\left(\beta - \frac{l_r}{v} r\right) \tag{4}$$

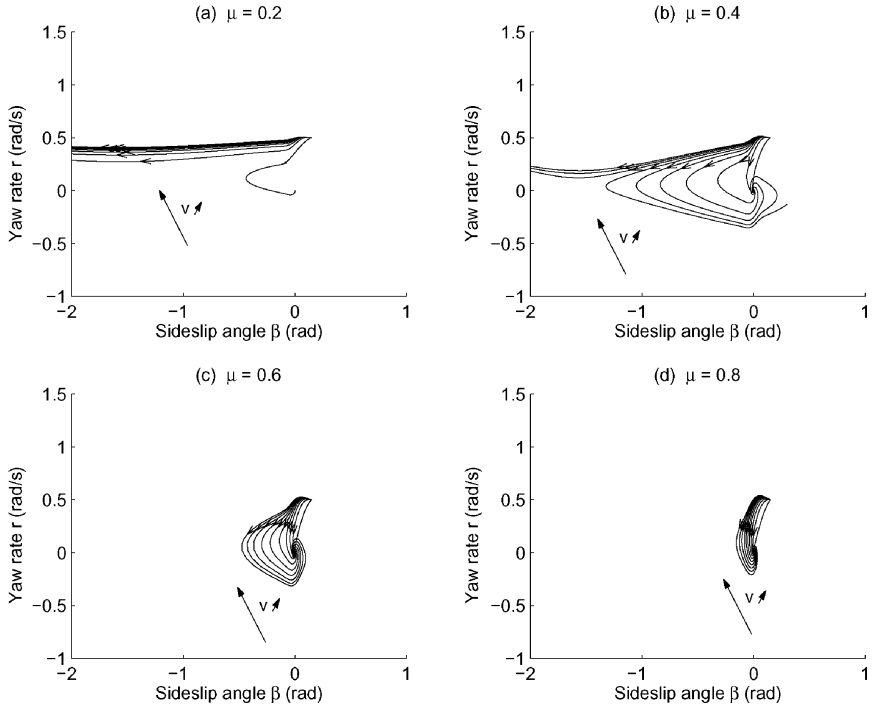

Fig. 5. Effect of speed and road adhesion on vehicle stability with $\delta_f = 0$ rad.

The nominal forward speed for controller synthesis is chosen as $v_0 = 20\,\mathrm{m/s}$. However v is considered as a varying parameters in the range $[1, 40]\,\mathrm{m/s}$. The derived model is of second order with state vector $\left(x = [\beta, r]^T\right)$, disturbance input $(w = f_w)$ and as control input, the steering angle $\left(u = \delta_f\right)$.

$$\dot{x} = Ax + B_w w + B_u u \tag{5}$$

where

$$A = \begin{bmatrix} -\dfrac{c_r + c_f}{mv} & -1 + \dfrac{l_r c_r - l_f c_f}{mv^2} \\ \dfrac{l_r c_r - l_f c_f}{J} & -\dfrac{l_r^2 c_r + l_f^2 c_f}{Jv} \end{bmatrix}, \qquad B_w = \begin{bmatrix} \dfrac{1}{mv} \\ \dfrac{l_w}{J} \end{bmatrix}, \qquad B_u = \begin{bmatrix} \dfrac{c_f}{mv} \\ \dfrac{c_f l_f}{J} \end{bmatrix} \tag{6}$$

Simulation of this model shows also that the speed and road adhesion variations affect both the transient and the steady state behavior of the vehicle in response

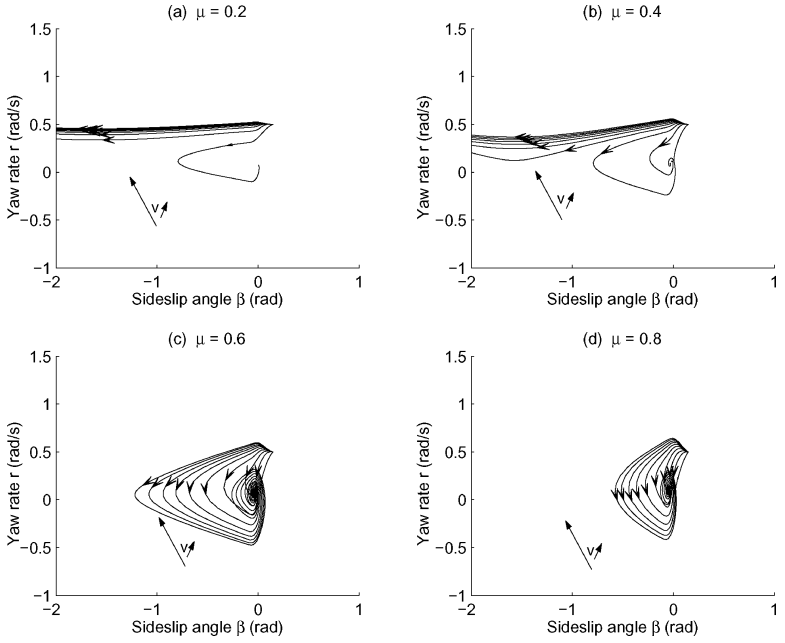

Fig. 6. Effect of speed and road adhesion variations on vehicle stability with $\delta_f = 0.05$ rad.

to driver steering angle input or lateral wind force input. Increasing speed and road adhesion reduction have the same effect and lead to damping reduction (Fig. 9).

The following section adopts a linear fractional transformation (LFT) modelling approach in order to take into account the possible separate variations of the cornering stiffnesses and forward speed.

2.4. Vehicle LFT Modelling

We assume the following parameter variations:

$$\begin{cases} c_f = c_{f0}(1 + \sigma_f \delta_1), & \|\delta_1\| \leq 1 \\ c_r = c_{r0}(1 + \sigma_r \delta_2), & \|\delta_2\| \leq 1 \\ v = v_0(1 + \sigma_v \delta_3), & \|\delta_3\| \leq 1 \end{cases} \tag{7}$$

The positive scaling factors σ_f, σ_r and σ_v are used to reflect the magnitude of the deviation from the nominal values c_{f0}, c_{r0} and v_0. In order to transform the parameter varying system (5) in the form of a minimal order LFT model, six fictitious inputs and

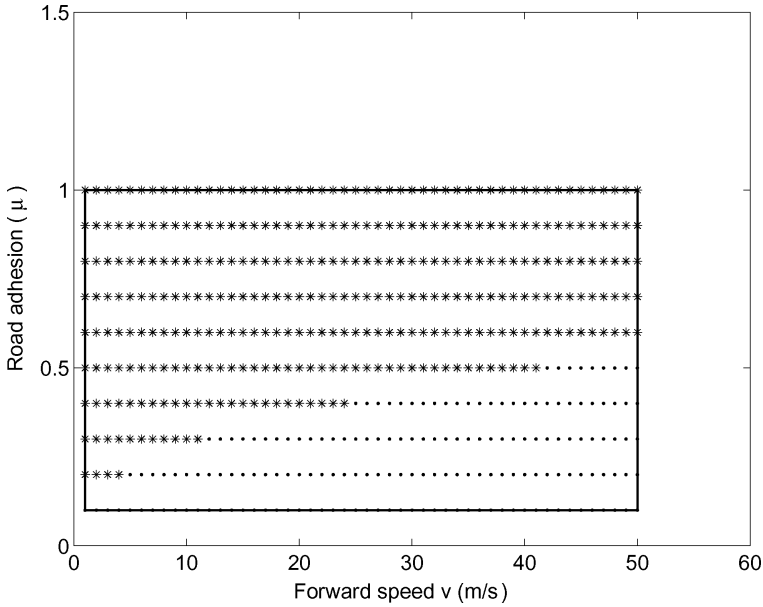

Fig. 7. Speed-road adhesion stability region with $\delta_f = 0.0$ rad for initial condition $[\beta_0, r_0]^T = [0.15, 0.5]^T$. "*" : stable points, "." unstable ones.

outputs are needed. One fictitious input and output for each cornering stiffnesses variation, and four fictitious inputs and outputs for the variation of the longitudinal speed. The fictitious input and output vectors are related by $(p = \Delta q)$, where the diagonal perturbation matrix is $\Delta = diag\{\delta_1, \delta_2, \delta_3, \delta_3, \delta_3, \delta_3\}$. After some algebra manipulations, the LFT model takes the following form, where the system output is chosen to be the yaw rate r.

$$\begin{bmatrix} \dot{x} \\ q \\ r \end{bmatrix} = \begin{bmatrix} A & B_p & B_w & B_u \\ C_q & D_{qp} & D_{qw} & D_{qu} \\ C_r & D_{rq} & D_{rw} & D_{ru} \end{bmatrix} \begin{bmatrix} x \\ p \\ w \\ u \end{bmatrix} \tag{8}$$

with $u = \delta_f$ and

$$A = \begin{bmatrix} a_{11} & a_{12} \\ a_{21} & a_{22} \end{bmatrix}, \qquad B_u = \begin{bmatrix} b_1 \\ b_2 \end{bmatrix}, \qquad B_w = \begin{bmatrix} h_1 \\ h_2 \end{bmatrix}$$

$$B_p = \begin{bmatrix} \dfrac{c_{f0}}{mv_0}\sigma_f & \dfrac{c_{r0}}{mv_0}\sigma_r & -2\sigma_v & -\sigma_v & 0 & 0 \\ \dfrac{c_{f0}l_f}{J}\sigma_f & -\dfrac{c_{r0}l_r}{J}\sigma_r & 0 & 0 & \sigma_v & 0 \end{bmatrix}$$

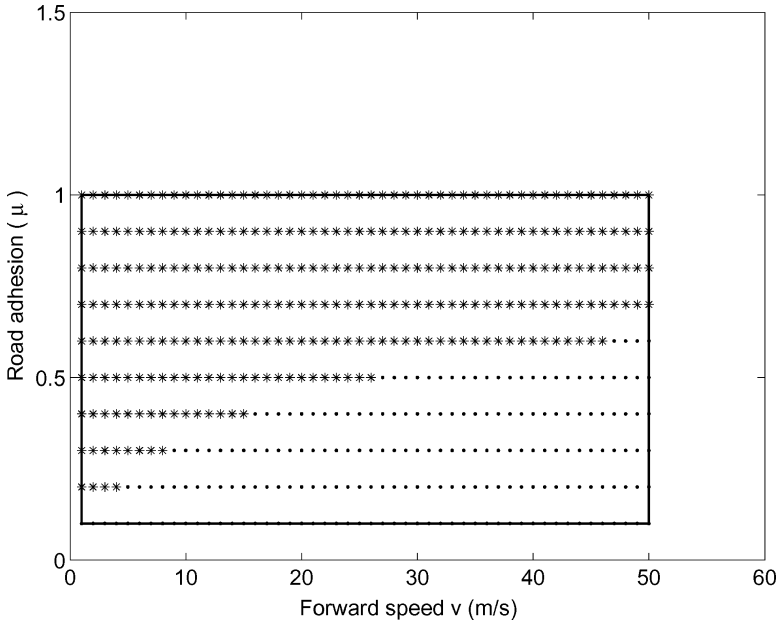

Fig. 8. Speed-road adhesion stability region with $\delta_f = 0.05$ rad for initial condition $[\beta_0, r_0]^T = [0.15, 0.5]^T$. "*" : stable points, "." unstable ones.

$$C_q = \begin{bmatrix} -1 & -\dfrac{l_f}{v_0} \\ -1 & \dfrac{l_r}{v_0} \\ 0 & (a_{12}+1) \\ a_{11} & 0 \\ 0 & -a_{22} \\ 0 & 1 \end{bmatrix}$$

$$D_{qp} = \begin{bmatrix} 0 & 0 & 0 & 0 & 0 & \dfrac{l_f}{v_0}\sigma_v \\ 0 & 0 & 0 & 0 & 0 & -\dfrac{l_r}{v_0}\sigma_v \\ 0 & 0 & -\sigma_v & 0 & 0 & 0 \\ \dfrac{c_{f0}}{mv_0}\sigma_f & \dfrac{c_{r0}}{mv_0}\sigma_r & -\sigma_v & -\sigma_v & 0 & 0 \\ 0 & 0 & 0 & 0 & -\sigma_v & 0 \\ 0 & 0 & 0 & 0 & 0 & -\sigma_v \end{bmatrix}$$

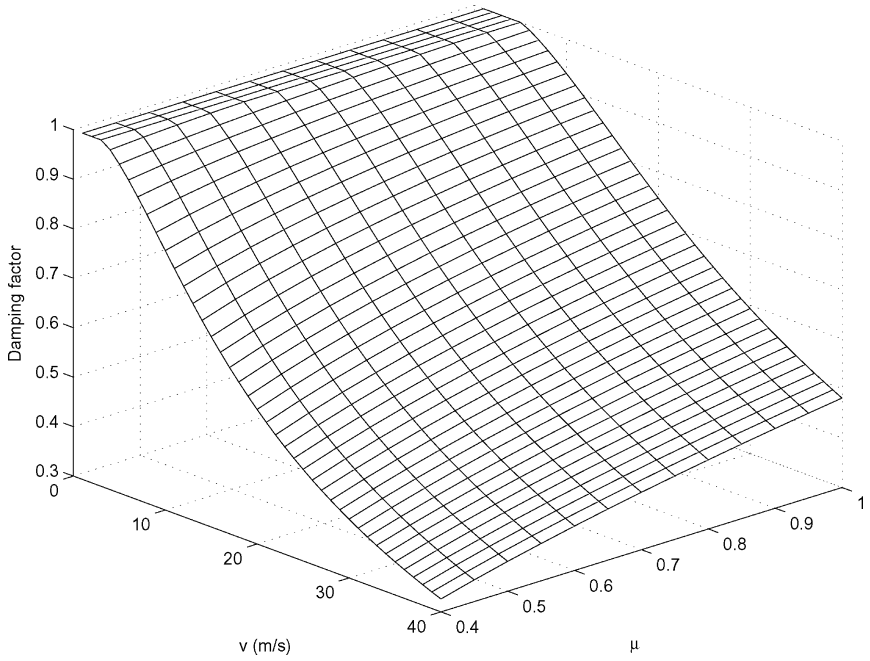

Fig. 9. Damping factor function of speed and road adhesion.

$$D_{qw} = \begin{bmatrix} 0 \\ 0 \\ 0 \\ h_1 \\ 0 \\ 0 \end{bmatrix}, \quad D_{qu} = \begin{bmatrix} 1 \\ 0 \\ 0 \\ b_1 \\ 0 \\ 0 \end{bmatrix}$$

where

$$a_{11} = -\frac{c_{r0} + c_{f0}}{m v_0} \quad a_{12} = -1 + \frac{l_r c_{r0} - l_f c_{f0}}{m v_0^2} \quad b_1 = \frac{c_{f0}}{m v_0}$$

$$a_{21} = \frac{l_r c_{r0} - l_f c_{f0}}{J} \quad a_{22} = -\frac{l_r^2 c_{r0} + l_f^2 c_{f0}}{J v_0} \quad b_2 = \frac{c_{f0} l_f}{J}$$

$$h_1 = \frac{1}{m v_0} \qquad h_2 = \frac{l_w}{J}$$

All other matrices of (8) are zero. Calculation details are given in the appendix. Finally the corresponding transfer matrix from $[p^T, w, u]^T$ to $[q^T, r]^T$ is denoted P (Fig. 10).

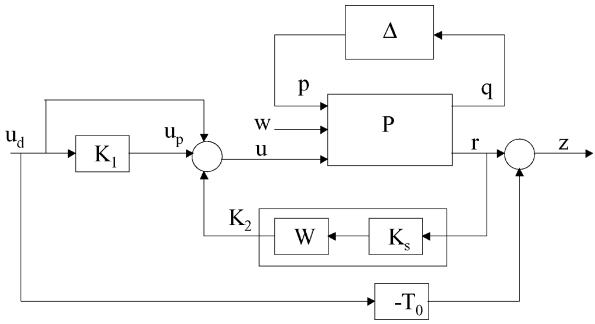

Fig. 10. Feedforward control with reference model.

3. ACTIVE STEERING DESIGN METHODOLOGY

The active steering method developed in this paper has to improve vehicle stability and handling while taking into account the driver steering command. The control objectives are then primarily quadrupled:

- enhancement of vehicle stability region by protecting it from spin under low adhesion roads;
- rejection of disturbances such as side wind force or yaw torque disturbances;
- in nominal situations, the vehicle has also to present similar steady state behavior as the conventional car without active steering;
- enhancement of the damping of vehicle responses for all operational speeds while ensuring similar transient behavior for all speeds and road adhesion.

The above four points summarize the needed vehicle handling improvement [17]. The first three objectives will be achieved using a control feedback from the yaw rate while the best candidate for identical transient behavior is robust model matching which is taken into account in two-degree-of-freedom control.

Considering vehicle active steering, the tire steering angle u is set in part by the driver through the vehicle classical steering mechanism while an additional steering angle δ_c is set by the controller using an hydraulic or a DC-motor actuators combined with a differential mechanical device [13, 14]. The tire steering angle is thus

$$u = u_d + \delta_c \tag{9}$$

where $u_d = \frac{\delta_d}{R}$, δ_d is the steering wheel angle set by the driver and R is the steering gear ratio.

The controller combines a feedforward and a feedback part, its output is thus divided into two parts K_1 and K_2 and takes the following form (Fig. 10)

$$\delta_c = K_1 u_d + K_2 r \tag{10}$$

Controller K_1 acts as a prefilter of the reference signal by adding the feedforward action $(u_p = K_1 u_d)$ while the feedback controller K_2 ensures robust stability of the feedback loop with guaranteed damping enhancement on the yaw rate. The third controller objective is fulfilled by making the vehicle yaw rate response to robustly follow as close as possible the response of a reference model. This fact constitutes robust model matching [15]. More precisely, let z be the difference between the vehicle yaw rate response and the response of the reference model. The feedforward part K_1 of the controller has to keep this error signal z small for an entire family of perturbed plants described by the previous LFT model. Finally the last control objective necessitates some speed scheduling of the controller and imposes a limitation on the controller time response. In fact it has to act during driver reaction time.

In the following, a two-stages approach is adopted. At the first stage the feedback part K_2 of the controller is computed using the H_∞ coprime based loop shaping method of [16]. Afterwards, the new vehicle model which incorporates the feedback controller is computed, thus the feedforward part K_1 is synthesized from a second H_∞ optimization.

3.1. Feedback Part Synthesis

Let $G(s)$ be the nominal transfer function from the steering angle to the yaw rate. In order to reject a constant step input perturbation on the yaw rate, a weighting compensator of the form of a 10 DC gain low pass filter is introduced, according to the loop shaping design methodology [16, 17].

$$W(s) = \frac{10}{10s + 1} \tag{11}$$

Let now G_s be the shaped plant $(G_s = WG)$, using normalized coprime description, one can write $G_s = \tilde{N}_s / \tilde{M}_s$. A stabilizing feedback controller K_s is directly computed using the procedure in [16] such that

$$\left\| \begin{bmatrix} I \\ K_s \end{bmatrix} (I - G_s K_s)^{-1} [I \quad G_s] \right\|_\infty \leq \gamma \tag{12}$$

with $\gamma = 1.1 \left\{ 1 - \left\| \begin{bmatrix} \tilde{N}_s & \tilde{M}_s \end{bmatrix} \right\|_H^2 \right\}^{-1/2}$ is a relaxed value of the maximal stability margin. This procedure needs to resolve two Riccati equations, but no iteration on γ is needed. For $\gamma = 2.3$, a state space representation of the obtained strictly proper controller is

$$K_s = \begin{bmatrix} A_s & C_s \\ B_s & D_s \end{bmatrix} = \left[\begin{array}{ccc|c} -4.476 & -75.091 & 26.229 & -74.159 \\ 17.198 & -1104.9 & 332.42 & -1100.4 \\ -3.321 & -165.03 & -70.256 & -158.01 \\ \hline 0.4152 & 9.8764 & 7.532 & 0 \end{array}\right] \tag{13}$$

In this particular procedure, the role of the controller K_s is to provide the needed phase lead for close loop stabilization. It is also well-known that according to the small gain theorem, this controller ensures robust stability for the family of perturbed plants

$$\Pi_{sp} = \left\{ \hat{G}_s / \hat{G}_s = (\tilde{M}_s - \Delta_{\tilde{M}_s})^{-1} (\tilde{N}_s + \Delta_{\tilde{N}_s}) \right\} \tag{14}$$

such that $\| [\Delta_{\tilde{M}_s} \Delta_{\tilde{N}_s}] \|_\infty < \gamma^{-1}$. The final implemented feedback controller is thus $K_2 = WK_s$ (Fig. 10).

3.2. Feedforward Part Synthesis

Since the wind force is rejected by the closed loop part of the controller, it will not be further considered for the feedforward part synthesis. The loop is closed by controller K_2 and system input reduces to $\left[p^T, u_d, u_p\right]^T$. Let now T_0 be the desired transfer function between u_d and r. In order to ensure at nominal speed, the same steady state value for the controlled and the conventional car, the reference model is chosen as a first order transfer function with the same steady state gain as the conventional car. It is of the form

$$T_0 = \frac{G(v_0)}{0.2s + 1} \tag{15}$$

The settling time is about 0.8 s. A first order model also avoids overshot on vehicle responses.

The feedforward part K_1 of the controller has to keep the error signal z small for an entire family of the LFT modeled perturbed plants. The error signal z is computed from $(z = r - T_0 u_d)$. The system of Figure 10 is thus updated to the one of Figure 11,

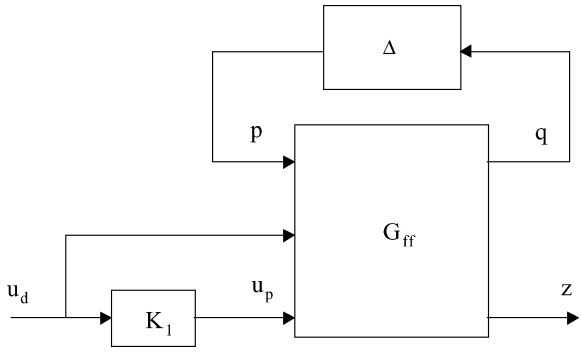

Fig. 11. Feedforward control.

where G_{ff} includes the reference model and is the transfer matrix from $\left[p^T, u_d, u_p\right]^T$ to $[q^T, z]^T$. The transfer function from driver input u_d to z is given by

$$T_{zu_d} = \mathcal{F}_u\left(G_{ff}\begin{bmatrix}1 & 0\\ 0 & 1\\ 0 & K_1\end{bmatrix}, \Delta\right) \tag{16}$$

where $\mathcal{F}_u$ stands for upper fractional transformation [6].

The control $u_p = K_1 u_d$ will be designed such as the H_∞ robust performance level γ_f is ensured

$$\sup_{\Delta\in\mathbf{B}_\Delta} \|T_{zu_d}\|_{\mathcal{L}_2\longrightarrow\mathcal{L}_2} < \gamma_f \tag{17}$$

where $\mathbf{B}_\Delta$ is the unit ball defined by $\mathbf{B}_\Delta = \{\Delta = diag\{\delta_1, \delta_2, \delta_3 I_4\}, \|\Delta\| \le 1\}$.

Assuming that a state-space realization of G_{ff} is given by

$$G_{ff}(s) = \left[\begin{array}{c|ccc} A_{cl} & B & E & M\\ \hline C_1 & L_1 & H_1 & N_1\\ C_2 & L_2 & H_2 & N_2\end{array}\right] \tag{18}$$

The condition for the existence of such controller is given by the 3 LMIs [1, 18]

$$\widetilde{\mathcal{M}}_R\begin{bmatrix} A_{cl}R + RA_{cl}^T & RC_1^T & RC_2^T & BX & E\\ C_1R & -X & 0 & L_1X & H_1\\ C_2R & 0 & -I & L_2X & H_2\\ XB^T & XL_1^T & XL_2^T & -X & 0\\ E^T & H_1^T & H_2^T & 0 & -\gamma_f^2 I\end{bmatrix}\widetilde{\mathcal{M}}_R^T < 0 \tag{19}$$

$$\begin{bmatrix} ZA_{cl}^T + A_{cl}Z & BX & ZC_1^T & ZC_2^T\\ XB^T & -X & XL_1^T & XL_2^T\\ C_1Z & L_1X & -X & 0\\ C_2Z & L_2X & 0 & -I\end{bmatrix} < 0 \tag{20}$$

$$R - Z \ge 0 \tag{21}$$

where $\widetilde{\mathcal{M}}_R = diag\{\widetilde{\mathcal{N}}_R, I\}$, and $\widetilde{\mathcal{N}}_R$ is a matrix whose columns constitute a basis of the kernel of $\begin{bmatrix} M^T & N_1^T & N_2^T\end{bmatrix}$, R and Z are symmetric definite matrices and X is a symmetric bloc-diagonal matrix which commutes with Δ. The controller is then reconstructed using classical H_∞ optimization [1]. The process is the following:

- form the matrices $Q = \begin{bmatrix} X^{\frac{1}{2}} & 0\\ 0 & I\end{bmatrix}$ and $Q_{\gamma_f} = \begin{bmatrix} X^{\frac{1}{2}} & 0\\ 0 & \gamma_f^{-1} I\end{bmatrix}$

- compute the state space form of the system G_Q given by

$$G_Q(s) = \left[\begin{array}{c|ccc} A_{cl} & BQ_{\gamma_f} & E & M \\ \hline Q^{-1}C_1 & Q^{-1}L_1Q_{\gamma_f} & Q^{-1}H_1Q_{\gamma_f} & Q^{-1}N_1 \\ 0 & 0 & Q_{\gamma_f} & 0 \end{array}\right] \tag{22}$$

- finally perform the H_∞ standard optimization (23) to get the feedforward controller K_1

$$\left\|F_l(G_Q, K_1)\right\|_\infty \leq 1 \tag{23}$$

where $\mathcal{F}_l$ stands for low fractional transformation [6].

In our case, the optimization procedure yields a $\gamma_f = 0.71$ and a 7 order controller given below in state space representation

$$K_1 = \left[\begin{array}{c|c} A_1 & C_1 \\ \hline B_1 & D_1 \end{array}\right] \tag{24}$$

$$= \left[\begin{array}{ccccccc|c} 455.6 & 49.55 & 93.00 & -147.3 & 2602 & 590.3 & -203.1 & -32.19 \\ 495.5 & -416.7 & -4508 & 734.1 & 2842 & -420.7 & 368.1 & -2.613 \\ 93 & -186.5 & -1702 & 272.9 & 1069 & -58.59 & 63.17 & -0.326 \\ -147.3 & 232.2 & 2320 & -498.3 & -1439 & 85.89 & -92.54 & 0.174 \\ 260.3 & -244 & -2593 & 447.1 & 1622 & -216.9 & 189.1 & -0.986 \\ 590.3 & 306.7 & 789.9 & -141.9 & -476.7 & -589.1 & 439.9 & 1.294 \\ -203.1 & -289.4 & -1695 & 283.6 & 1056 & 215.0 & -159.7 & -27.36 \\ \hline -32.19 & -11.79 & -0.492 & -7.184 & 0.955 & 29.15 & -22.24 & 0 \end{array}\right] \tag{25}$$

3.3. Controller Implementation

The controller is finally implemented as shown on Figure 12. The weighting filter W is included in the feedback controller K_2. Disturbances are thus filtered. However, in order to obtain a similar steady state behavior for the conventional and the controlled

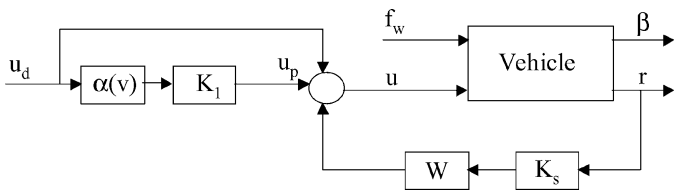

Fig. 12. Active steering controller implementation.

car, a speed scheduled gain $\alpha(v)$ has to be added to the prefilter part K_1. The gain is computed form

$$\alpha(v) = \frac{G(v)W(0)K_s(0)}{K_1(0)} \tag{26}$$

which makes the DC gain of the transfer function T_{ru_d} from u_d to r (Fig. 12) equal to the one of the conventional car $G(v)$.

The controller implementation needs three types of measurements: measurement of the yaw rate by a gyro, the speed by an tachometer and the steering wheel angle by an encoder.

4. SIMULATION RESULTS

All the simulations are conducted on the nonlinear model. In all figures, solid lines correspond to the controlled car responses and dotted ones to the conventional car responses.

4.1. Stability Domain Enhancement

First of all, in order to quantify the stability enhancement by the feedback controller alone, it is supposed that the driver steering angle is zero. The feedforward action in this case is also zero. The initial conditions of the controlled vehicle are the same as those taken for Figure 5, speed and road adhesion values are also the same. Results are given in Figure 13. It is easy to see from this figure that all trajectories of the controlled vehicle are now stable, this is to strengthened by the fact that all tested points in the previous rectangular area of the adhesion-speed plane (Fig. 7) are now stable. As an example, the vehicle at $\mu = 0.2$ is stable for all considered speeds.

4.2. Disturbance Rejection

The vehicle is supposed to be at nominal speed and full road adhesion and is subject to a step disturbance wind force. The wind force appears at time $t_1 = 1$ s and disappears at $t_2 = 2$ s. It is assumed that the driver does not react to this disturbance ($u_d = \frac{\delta_d}{R} = 0$). One can note from Figure 14 that the yaw rate is greatly reduced and thus the controlled vehicle will remain closer to road centerline. In addition, the maximum value of yaw rate during the transient phase is smaller than the one of the conventional car and the disturbance is practically rejected within driver reaction time.

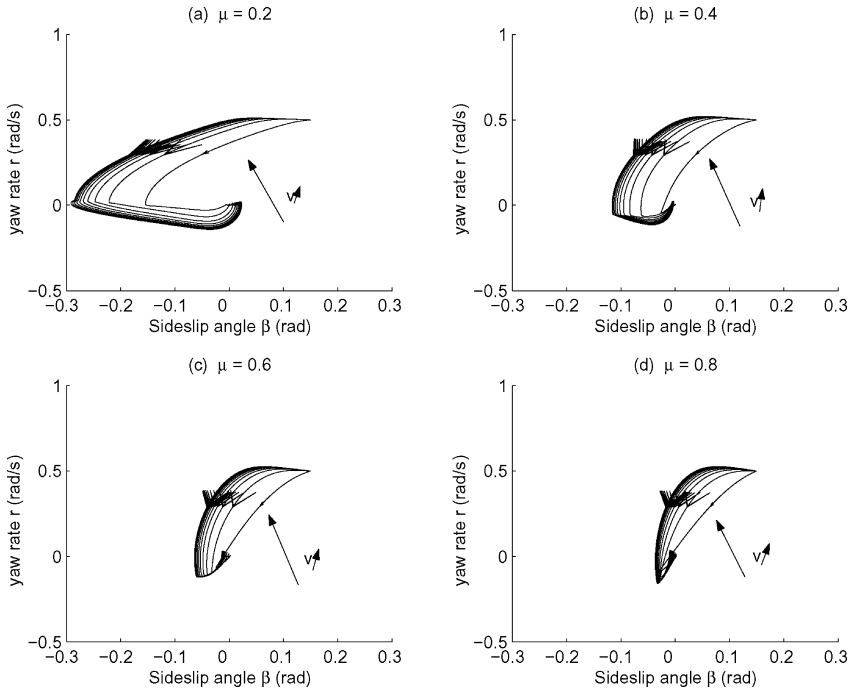

Fig. 13. Effect of speed and road adhesion on controlled vehicle stability with no driver action.

Responses for $v = 30\,\text{m/s}$ and $\mu = 0.5$ are given in Figure 15. The controller exhibits good stability and performance robustness, in fact responses are still well damped.

4.3. Lane Change Maneuver

The handling improvement is now investigated in case of driver steering angle which corresponds to lane change maneuver (Fig. 16c, dotted line). The dashed-dot line corresponds to the response of the reference model. Figure 16 shows results obtained at nominal speed with road adhesion equal to 1. Figure 17 shows results obtained for $v = 40\,\text{m/s}$ and $\mu = 1$. Due to the speed scheduling of the gain parameter $\alpha(v)$, we ensure that the controlled vehicle and the conventional one present the same steady state behavior.

On the other hand, the controlled yaw rate response of the controlled car closely follows the response of the reference model T_0. Responses are degraded for high speed and low road adhesion values ($v = 40\,\text{m/s}$ and $\mu = 0.5$), however, they

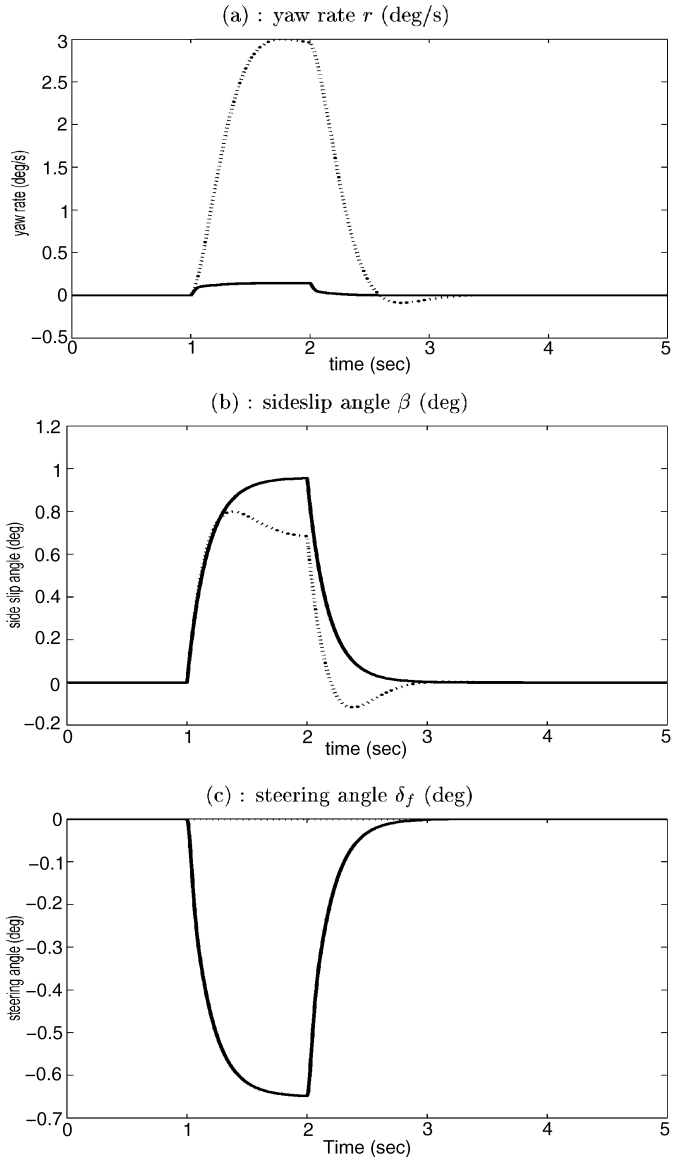

Fig. 14. Wind forces step input rejection for nominal system (solid: controlled, dotted: conventional).

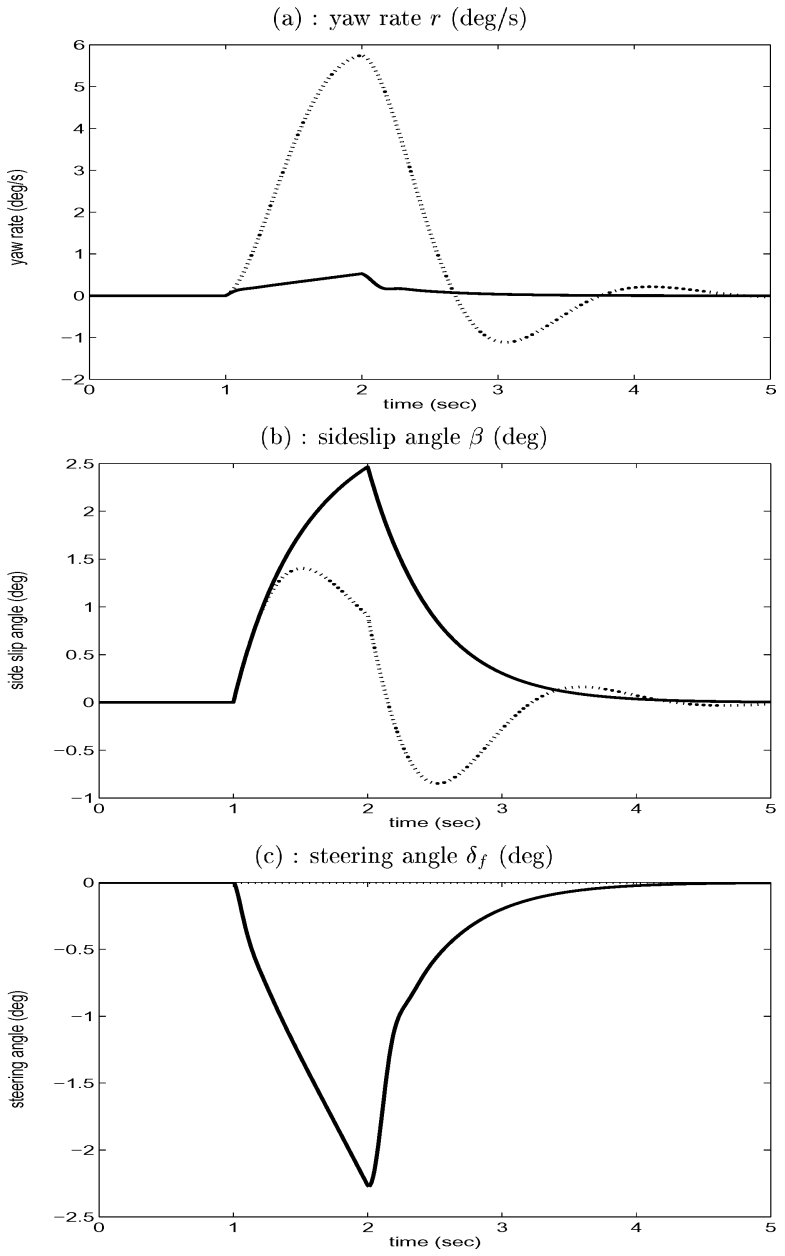

Fig. 15. Wind forces step input rejection for $v = 30$ m/s and $\mu = 0.5$ (solid: controlled, dotted: conventional).

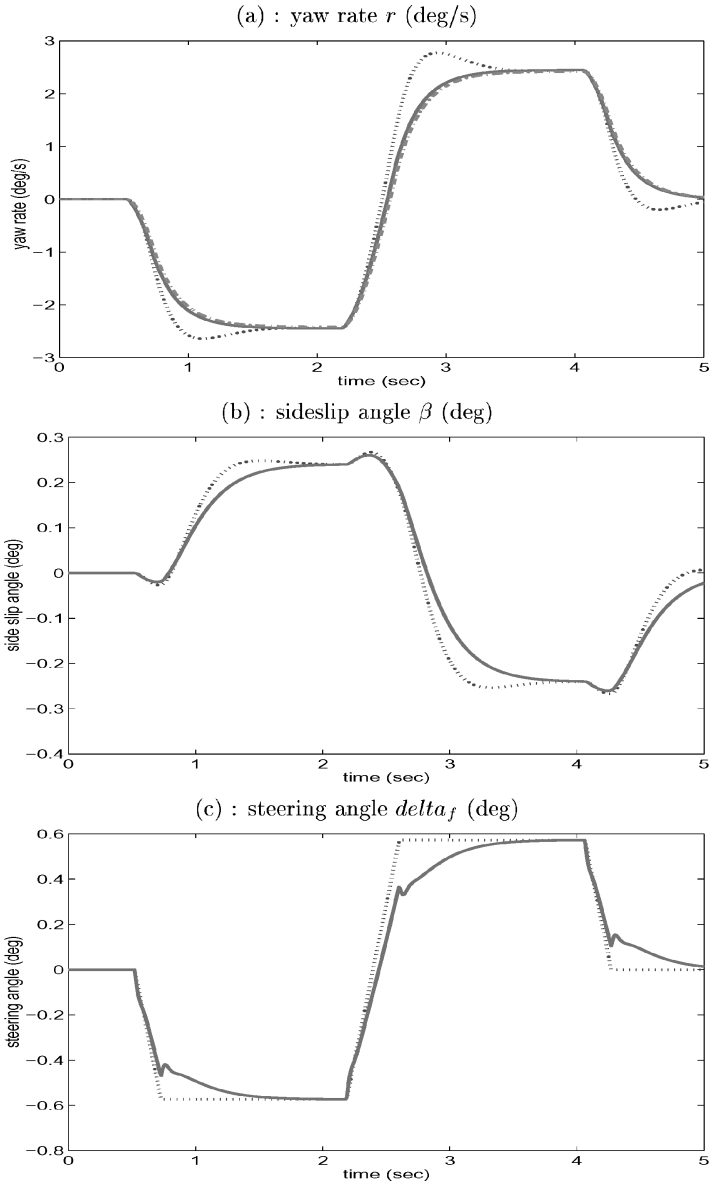

Fig. 16. Lane change maneuver, nominal system (solid: controlled, dotted: conventional, dashed: reference model).

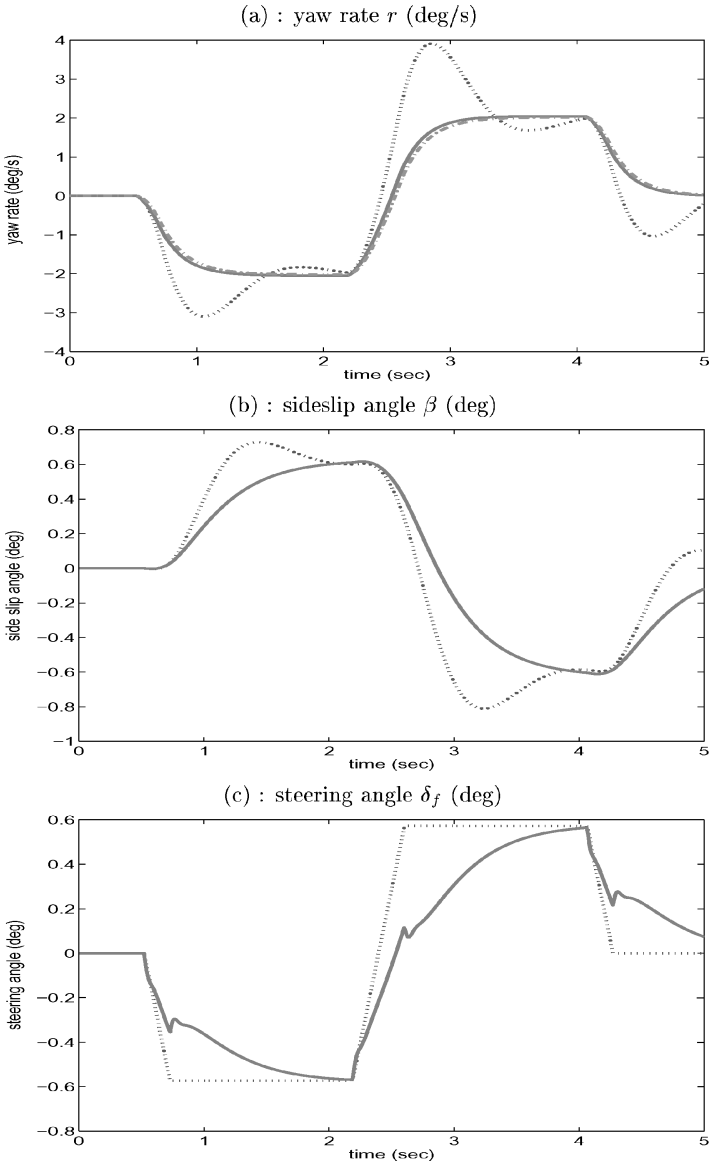

Fig. 17. Lane change maneuver, for nominal road adhesion and speed at 40 m/s (solid: controlled, dotted: conventional, dashed: reference model).

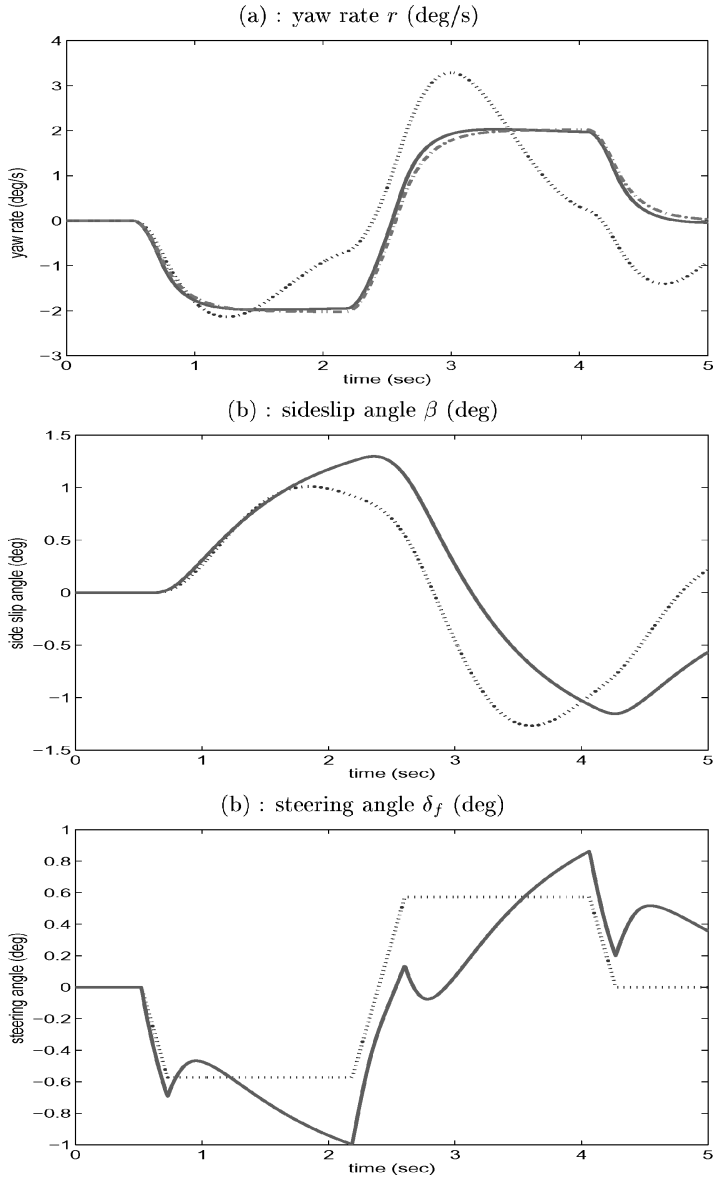

Fig. 18. Lane change maneuver for $v = 40\,\text{m/s}$ and $\mu = 0.5$ (solid: controlled, dotted: conventional, dashed: reference model).

practically do not present overshot (Fig. 18). The robust model matching of the previous section makes the controlled vehicle to robustly follow the specified first order reference model T_0. Figures show also a reduction of sideslip angle during the transient phase (Figs. 16b and 17b). One can notice that the control effort is limited (Figs. 16c to 18c). The controller subtracts or adds a steering angle to the driver command. When the road adhesion is at its nominal value even when the speed varies, the control effort vanishes within driver reaction time which is assumed to be between 0.5 and 1 s. When the road adhesion is decreased, there is a remaining steering angle.

4.4. Aquaplaning Maneuver

In this case, the vehicle is considered to perform a stationary cornering maneuver at 40 m/s. The driver steering angle is then constant. It is also assumed that at $t = 2$ s, the left front tire crosses a low friction region of the road, a stain of oil for example, while the three other tires remain on high friction. The tire returns to a dry road at 2.5 s. It is further assumed that the driver does not react to this situation.

Figure 19a shows that the controlled car recovers the reference model response within the driver reaction time. Sideslip angle variations are limited (Fig. 19b). Additional lateral forces are generated using the steered tires (Fig. 19c).

In Figure 20 appears the path that would be followed by the vehicle in case of no aquaplaning and the paths of the three vehicles (conventional, controlled, model reference) in the case of normal adhesion and aquaplaning. One can notice that the path of the controlled vehicle is the closest to the path in non aquaplaning situation while the conventional vehicle lateral deviation is greater than the lane width so a lane departure may be expected.

Finally, Figure 21 displays the perpendicular distances between the paths of the different vehicles. After 5 s, in normal condition (no aquaplaning), the distance between the controlled car and the reference one is less than 10 cm. This distance is about 27 cm when an aquaplaning occurs. In comparison, the conventional vehicle path during aquaplaning maneuver, deviates about 2.6 m from its path in normal conditions.

5. CONCLUSION

In this paper, some stability aspects of lateral motion of a vehicle are discussed. It is shown that vehicle stability depends on several parameters. Therefore, a certain initial state condition and a constant steering angle are assumed. As an example a stability region is constructed as a function of road adhesion and speed. Afterwards, an active steering method is developed using a combination of feedforward and feedback

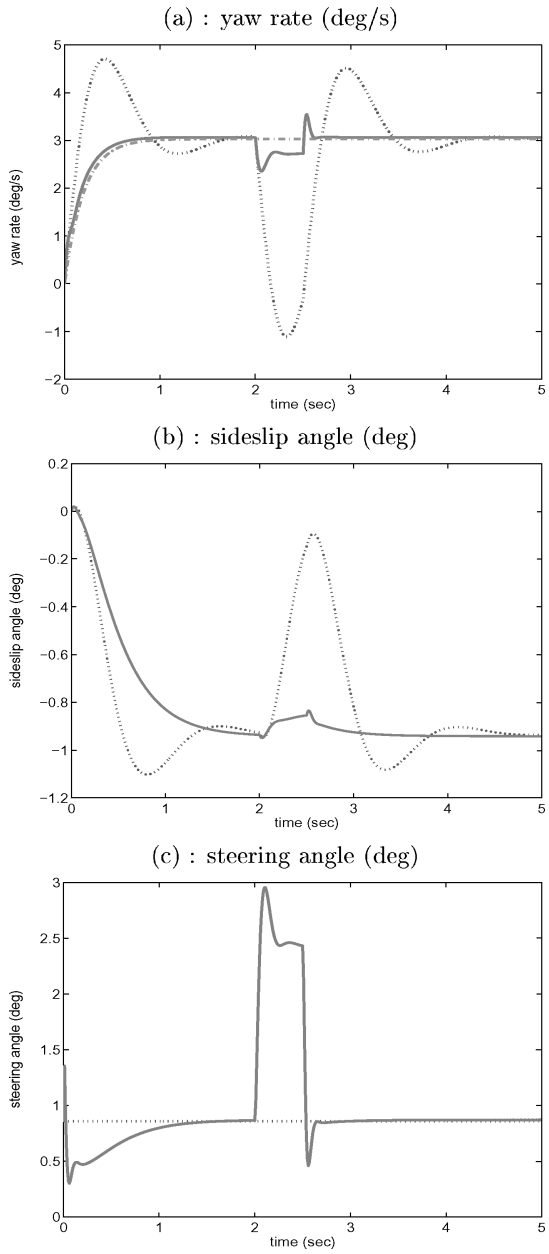

Fig. 19. Aquaplaning maneuver (solid: controlled, dotted: conventional, dashed: reference model).

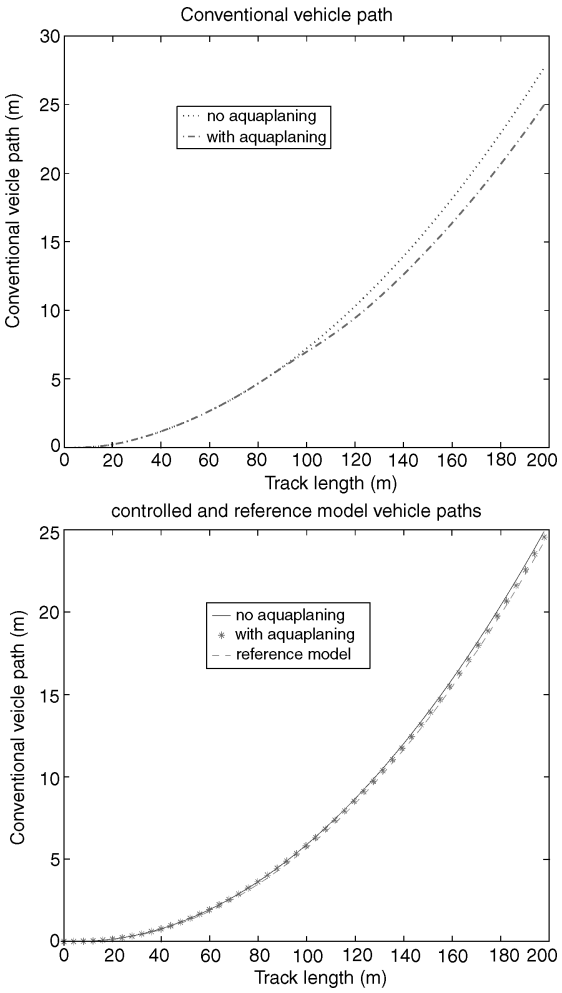

Fig. 20. Path of the different vehicles.

H_∞ controllers with main objective vehicle handling improvement. The synthesis methodology simply allows direct specification of time domain objectives such as reference model matching. The obtained controller is tested on three typical maneuvers. The controller exhibits good performances and robustness properties face to parameters variations and enhances overall vehicle stability.

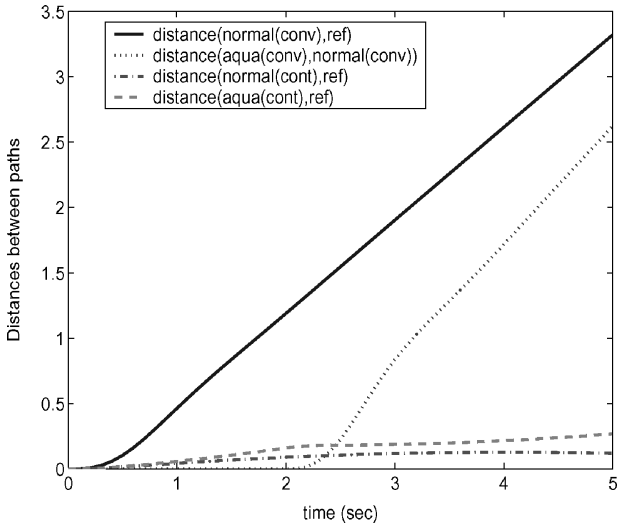

Fig. 21. Distances between the paths of the different vehicles.

REFERENCES

1. Giusto, A. and Paganini, F.: Robust Synthesis of Feedforward Compensators. *IEEE Transactions on Automatic Control* 44 (1999), pp. 1578–1582.
2. Ackermann, J. and Odenthal, D.: Robust Steering Control for Active Rollover Avoidance of Vehicles with Elevated Center of Gravity. *International Conference on Advances in Vehicle Control and Safety*, Amiens, France, 1998, pp. 118–123.
3. Ackermann, J. and Bünte, T.: Handling Improvement for Robustly Decoupled Car Steering Dynamics. *4th IEEE Mediterranean Symposium on New Directions in Control & Automation*, Chania, Greece, 1996.
4. Ackermann, J. and Bünte, T.: Handling Improvement of Robust Car Steering. *International Conference on Advances in Vehicle Control and Safety*, Amiens, France, 1998.
5. Mammar, S.: Robust Automatic Steering Using Fuzzy Modelling and LMI Control. *IFAC Conference on System Structure and Control*, Nantes, France, 1998.
6. Doyle, J.C., Zhou, K. and Glover, K.: *Robust and Optimal Control*. Prentice Hall, first edition, 1996.
7. Pacejka, H.B.: Tire Factors and Vehicle Handling. *Int. J. Vehicle Design* 1 (1979), pp. 1–23.
8. Gim, G. and Nikravesh, P.E.: An Analytical Model of Pneumatic Tyres for Vehicle Dynamic Simulations. Part 1: Pure Slips. *Int. J. of Vehicle Design* 11(6) (1990), pp. 589–618.
9. Bonald, T., Bliman, P.A. and Sorine, M.: *Hysteresis Operators and Tire Friction Models: Application to Vehicle Dynamic Simulator.* Prof. of ICIAM., Hambourg, Germany, 1995.
10. Pacejka, H.B., Bakker, E. and Lidner, L.: A new Tire Model with an Application in Vehicle Dynamics Studies. In: *Proc. Int. Congress and Exposition*, *SAE* paper 890087, Detroit, Michigan, 1989.
11. Tuan, H.D., Ono, E., Hosoe, S. and Doi, S.: Bifurcation in Vehicle Dynamics and Robust Front Wheel Steering Control. *IEEE Transactions on Control Systems Technology* 6 (1998), pp. 412–421.

12. Kaesbauer, D., Sienel, W., Ackermann, J., Bartlett, A. and Steinhauser, R.: *Robust Control: Systems with Uncertain Physical Parameters*. Springer, London, 1993.
13. Ackermann, J., Odenthal, D. and Bünte, T.: Advantages of Active Steering for Vehicle Dynamics Control. *32nd International Symposium on Automotive Technology and Automation*, Vienna, Austria, 1999, pp. 263–270.
14. Balàza, M., Gombert, B., Hirzinger, G. and Willberg, B.: Planetary Roller Screw Drive. *32nd International Symposium on Automotive Technology and Automation*, European Production Engineering 19-3 (1995), pp. 28–29.
15. Kasenally, E.M., Limebeer, D.J.N. and Perkins, D.: On the Design of Robust Two Degree of Freedom Controllers. *Automatica* 29(1) (1993), pp. 157–168.
16. McFarlane, D. and Glover, K.: A Loop Shaping Design Procedure Using H_∞ Synthesis. *IEEE Transactions on Automatic Control* 37 (1992), pp. 759–769.
17. Mammar, S.: Two-Degree-of-Freedom Formulation of Vehicle Handling Improvement by Active Steering. *American Control Conference*, Chicago, Michigan, 2000.
18. Laub, A.J., Gahinet, P., Nemirovski, A. and Chilali, M.: LMI Control Toolbox. *The MathWorks*, 1995.

APPENDIX

The LFT model is obtained by considering for each state space equation the variation of cornering stiffnesses and speed respectively.

Cornering Stiffness Variations

Using Equation (7) and the single track model, one can write

$$\dot{\beta} = -r + c_{r0}\left(\frac{-1}{mv}\beta + \frac{l_r}{mv^2}r\right) + c_{f0}\left(\frac{-1}{mv}\beta + \frac{1}{mv}u - \frac{l_f}{mv^2}r\right) + \frac{c_{f0}}{mv}\sigma_f\delta_1\left(-\beta + u - \frac{l_f}{v}r\right) + \frac{c_{r0}}{mv}\sigma_r\delta_2\left(-\beta + \frac{l_r}{v}r\right) + \frac{1}{mv}w$$

and

$$\dot{r} = c_{r0}\left(\frac{l_r}{J}\beta - \frac{l_r^2}{Jv}r\right) + c_{f0}\left(\frac{-l_f}{J}\beta - \frac{l_f^2}{Jv}r + \frac{l_f}{J}u\right) + \frac{c_{f0}l_f}{J}\sigma_f\delta_1\left(-\beta - \frac{l_f}{v}r + u\right) + \frac{c_{r0}l_r}{J}\sigma_r\delta_2\left(\beta - \frac{l_r}{v}r\right) + \frac{l_w}{J}w$$

Thus define the fictitious outputs q_f, q_r as

$$\begin{cases} q_f = \left(-\beta + u - \dfrac{l_f}{v}r\right) \\ q_r = \left(-\beta + \dfrac{l_r}{v}r\right) \end{cases} \tag{27}$$

and the related fictitious inputs $\left(p_f = \delta_1 q_f\right)$ and $(p_r = \delta_2 q_r)$, one can thus write

$$\dot{\beta} = -\frac{c_{r0} + c_{f0}}{mv}\beta + \left(-1 + \frac{c_{r0}l_r - c_{f0}l_f}{mv^2}\right)r + \frac{c_{f0}}{mv}u + \frac{c_{f0}}{mv}\sigma_f p_f + \frac{c_{r0}}{mv}\sigma_r p_r + \frac{1}{mv}w$$

and

$$\dot{r} = a_{21}\beta + \left(-\frac{c_{r0}l_r^2 + c_{f0}l_f^2}{Jv}\right)r + b_2 u + b_2\sigma_f p_f - \frac{c_{r0}l_r}{J}\sigma_r p_r + h_2 w$$

Speed variations are now considered.

Speed Variations

Using the third line of Equation (7), one can arrive first to

$$\dot{\beta} = -r + \frac{1}{(1+\sigma_v\delta_3)}\left(\begin{array}{c}\dfrac{-(c_{r0}+c_{f0})}{mv_0}\beta + \dfrac{c_{f0}}{mv_0}u + \dfrac{c_{f0}}{mv_0}\sigma_f p_f + \dfrac{c_{r0}}{mv_0}\sigma_r p_r \\ + \dfrac{1}{mv_0}w + \dfrac{1}{(1+\sigma_v\delta_3)}\left(\dfrac{(c_{r0}l_r - c_{f0}l_f)}{mv_0^2}r\right)\end{array}\right)$$

using the fictitious input p_{v1} and the related output q_{v1} which is defined by

$$q_{v1} = \frac{1}{(1+\sigma_v\delta_3)}\left(\frac{c_r l_r - c_f l_f}{mv_0^2}r\right)$$

using the fact that $p_{v1} = \delta_3 q_{v1}$, one can get from the previous equation

$$q_{v1} = \left(\frac{c_r l_r - c_f l_f}{mv_0^2}r\right) - \sigma_v p_{v1} \tag{28}$$

and

$$\begin{aligned}\dot{\beta} = &\frac{1}{(1+\sigma_v\delta_3)}\left(a_{11}\beta + b_1 u + b_1\sigma_f p_f + \frac{c_{r0}}{mv_0}\sigma_r p_r + h_1 w - \sigma_v p_{v1}\right) \\ &+ a_{12}r - \sigma_v p_{v1}\end{aligned}$$

Using the same process as before, define q_{v2} and $p_{v2} = \delta_3 q_{v2}$ such as

$$\begin{cases} q_{v2} = \dfrac{1}{(1+\sigma_v\delta_3)}\left(a_{11}\beta + b_1 u + b_1\sigma_f p_f + \dfrac{c_{r0}}{mv_0}\sigma_r p_r + h_1 w - \sigma_v p_{v1}\right) \\ q_{v2} = \left(a_{11}\beta + b_1 u + b_1\sigma_f p_f + \dfrac{c_{r0}}{mv_0}\sigma_r p_r + h_1 w - \sigma_v p_{v1}\right) - \sigma_v p_{v2} \end{cases} \tag{29}$$

The final differential equation for β is

$$\begin{aligned}\dot{\beta} = &a_{11}\beta + a_{12}r + b_1 u + h_1 w \\ &+ b_1\sigma_f p_f + \frac{c_{r0}}{mv_0}\sigma_r p_r - 2\sigma_v p_{v1} - \sigma_v p_{v2}\end{aligned} \tag{30}$$

The procedure is the same for the yaw rate differential equation. One can define p_{v3} and q_{v3} such that $p_{v3} = \delta_3 q_{v3}$ and

$$q_{v3} = \left(\frac{c_r l_r^2 + c_f l_f^2}{Jv_0}r\right) - \sigma_v p_{v3} \tag{31}$$

to achieve

$$\begin{aligned}\dot{r} &= a_{21}\beta + a_{22}r + b_2u + h_2w \\ &\quad + \frac{c_{f0}l_f}{J}\sigma_f p_f - \frac{c_{r0}l_r}{J}\sigma_r p_r + \sigma_v p_{v3}\end{aligned} \tag{32}$$

As q_f and q_r, given in Equation (27) are speed depend, one needs to rewrite

$$\begin{cases} q_f = -\beta + u - \dfrac{1}{(1+\sigma_v\delta_3)}\dfrac{l_f}{v_0}r \\ q_r = -\beta + \dfrac{1}{(1+\sigma_v\delta_3)}\dfrac{l_r}{v_0}r \end{cases} \tag{33}$$

thus define p_{v4} and q_{v4} such that $p_{v4} = \delta_3 q_{v4}$ and

$$q_{v4} = r - \sigma_v p_{v4} \tag{34}$$

which achieves to

$$\begin{cases} q_f = -\beta + u - \dfrac{l_f}{v_0}(r - \sigma_v p_{v4}) \\ q_r = -\beta + \dfrac{l_r}{v_0}(r - \sigma_v p_{v4}) \end{cases} \tag{35}$$

The LFT model (Equation 8) is finally obtained by defining

$$\begin{cases} p = [\,p_f \quad p_r \quad p_{v1} \quad p_{v2} \quad p_{v3} \quad p_{v4}\,]^T \\ q = [\,q_f \quad q_r \quad q_{v1} \quad q_{v2} \quad q_{v3} \quad q_{v4}\,]^T \end{cases} \tag{36}$$